OXFORD

Cerebral Cortex, 2023, **33**, 2200–2214
https://doi.org/10.1093/cercor/bhac202
Advance access publication date 21 May 2022
Original Article

Network-specific selectivity of functional connections in the neonatal brain

Chad M. Sylvester[1,*], Sydney Kaplan[2], Michael J. Myers[1], Evan M. Gordon[3], Rebecca F. Schwarzlose[1], Dimitrios Alexopoulos[2], Ashley N. Nielsen[2], Jeanette K. Kenley[2], Dominique Meyer[2], Qiongru Yu[4], Alice M. Graham[5], Damien A. Fair[6], Barbara B. Warner[7], Deanna M. Barch[1,3,8], Cynthia E. Rogers[1,7], Joan L. Luby[1], Steven E. Petersen[2], Christopher D. Smyser[2,3,7]

[1]Department of Psychiatry, Washington University, 660 S. Euclid Avenue, St. Louis, MO 63110, USA,
[2]Department of Neurology, Washington University, 660 S. Euclid Avenue, St. Louis, MO 63110, USA,
[3]Department of Radiology, Washington University, 660 S. Euclid Avenue, St. Louis, MO 63110, USA,
[4]Joint Doctoral Program in Clinical Psychology, San Diego State University/University of California San Diego, 6363 Alvarado Court, Suite 103, San Diego, CA 92120, USA,
[5]Department of Psychiatry, Oregon Health and Science University, 3181 SW Sam Jackson Park Road, Portland, OR 97239, USA,
[6]Masonic Institute for the Developing Brain, Department of Pediatrics, and Institute of Child Development, University of Minnesota, 2025 E. River Parkway, Minneapolis, MN 55414, USA,
[7]Department of Pediatrics, Washington University, 660 S. Euclid Avenue, St. Louis, MO 63110, USA,
[8]Department of Psychological and Brain Sciences, Washington University, 660 S. Euclid Avenue, St. Louis, MO 63110, USA
*Corresponding author: Department of Psychiatry, Washington University, 660 S. Euclid, Campus Box 8511, St. Louis, MO 63110, United States.
Email: chad.sylvester@wustl.edu

The adult human brain is organized into functional brain networks, groups of functionally connected segregated brain regions. A key feature of adult functional networks is long-range selectivity, the property that spatially distant regions from the same network have higher functional connectivity than spatially distant regions from different networks. Although it is critical to establish the status of functional networks and long-range selectivity during the neonatal period as a foundation for typical and atypical brain development, prior work in this area has been mixed. Although some studies report distributed adult-like networks, other studies suggest that neonatal networks are immature and consist primarily of spatially isolated regions. Using a large sample of neonates ($n = 262$), we demonstrate that neonates have long-range selective functional connections for the default mode, fronto-parietal, and dorsal attention networks. An adult-like pattern of functional brain networks is evident in neonates when network-detection algorithms are tuned to these long-range connections, when using surface-based registration (versus volume-based registration), and as per-subject data quantity increases. These results help clarify factors that have led to prior mixed results, establish that key adult-like functional network features are evident in neonates, and provide a foundation for studies of typical and atypical brain development.

Key words: neonate; infant; networks; fMRI; functional connectivity.

Introduction

An important organizing principle of the adult human brain is that it can be divided into functional brain networks, distributed sets of brain regions that work together to perform specific types of processing (Raichle 2011). Prior work describing functional networks in neonates has been mixed (Fransson et al. 2007, 2009; Gao et al. 2009; Doria et al. 2010; Smyser et al. 2010; Gao et al. 2013; De Asis-Cruz et al. 2015; Gao et al. 2015; van den Heuvel et al. 2015; Gao et al. 2016; Smyser et al. 2016; Keunen et al. 2017). Although some studies report adult-like functional networks during the neonatal period, other studies have reported that functional networks during the neonatal period are immature and consist primarily of spatially isolated rather than distributed regions. The status of functional brain networks near birth is important for characterizing typical and atypical brain development and understanding which features of human brain organization might be impacted by the ex-utero environment. The current study utilizes a novel dataset of $n = 262$ neonates to identify sources contributing to the mixed findings in prior work and to comprehensively characterize neonatal functional brain networks.

Functional brain network organization is commonly measured with resting-state functional connectivity, correlations in activity measured with fMRI (Biswal et al. 1995). A defining feature of adult network organization is selectivity in long-range functional connections: spatially distant regions within the same network are more strongly functionally connected than spatially distant regions from different networks. For example, in adults, the portion of the lateral parietal cortex that is within the default mode network (DMN) is more strongly functionally connected to spatially distant regions in the superior frontal gyrus that are also within the DMN than to nearby regions in the frontal lobe from the dorsal attention network (DAN). Although a few prior studies provide evidence for long-range selective functional connections that may represent the DMN in neonates

Received: February 22, 2022. **Revised:** April 28, 2022. **Accepted:** April 29, 2022

(Doria et al. 2010; Smyser et al. 2010; Smyser et al. 2016; Keunen et al. 2017; Molloy and Saygin 2022), there is less evidence supporting long-range selective neonatal functional connections for other networks such as the DAN or the fronto-parietal network (FPN). Thus, some current models hypothesize that functional networks are relatively immature during the neonatal period and that adult-like networks emerge over the first years of life as short-range functional connections become weaker and long-range functional connections become stronger and more selective (Gao et al. 2016; Grayson and Fair 2017; Zhang et al. 2019).

Technical and methodological challenges may have contributed to the apparent immaturity of the neonatal brain. First, the standard practice of aligning infants to a common volume-based atlas may result in heterogeneity in the functional identity of individual voxels due to variation in gyral patterns across neonates (Hill et al. 2010). This challenge can be addressed with surface-based registration (Fischl et al. 1999), which permits nonlinear alignment of gyral patterns across participants. A second challenge is that infant blood-oxygen-level dependent (BOLD) images have unique sources of noise relative to older samples (Smyser and Neil 2015), which can be partly overcome by acquiring higher amounts of imaging data per subject. A final challenge is that short-range functional connectivity is high in neonates (Shi et al. 2017). As a result, studies that use nonlinear techniques to highlight the strongest functional connections in the neonatal brain (such as seed-based functional connectivity maps set to a particular threshold) are not designed to illustrate the weaker long-range functional connections. Similarly, network-detection techniques such as independent component analysis (ICA) may be dominated by the strong short-range functional connections and thus not designed to specifically test whether the long-range functional connections in neonates are network-selective. This challenge can be addressed by directly testing whether long-range selective functional connections exist in neonates (without using network-detection algorithms).

The goal of this study was to characterize the functional network organization of the neonatal brain and test the hypothesis that neonates exhibit long-range network-specific functional connections. To achieve these goals, we utilized a novel dataset (eLABE, $n = 262$) that included high amounts of data per participant (10–30 min of low-motion data) with surface-based registration of subjects. We first characterized whole-brain and seed-based functional connectivity in neonates in comparison with samples of children ($n = 61$, mean 10.5 years) and adults ($n = 120$, mean 25 years). Next, we quantified the specificity of both long- and short-range neonatal functional connections for same versus different functional networks. We then used 2 different network-detection algorithms to empirically define neonatal functional networks. Finally, we tested the extent to which surface-based registration (versus volume-based) and per-subject data quantity impact the apparent maturity of neonatal network organization. Results provide novel insights into the functional organization of the neonatal brain.

Materials and methods

Sample

This study was approved by the Human Studies Committees at Washington University in St. Louis and informed consent was obtained from mothers of neonatal participants. Mothers were recruited during the 2nd or 3rd trimester from 2 obstetrics clinics at Washington University as part of the Early Life Adversity, Biological Embedding, and Risk for Developmental Precursors of Mental Disorders (eLABE) study. The current study focused on imaging of offspring performed shortly after birth in full-term, healthy neonates (average PMA of included subjects 41.4 weeks, range 38–45). Neuroimaging data were collected between September 2017 and March 2020.

Inclusion criteria for the current study included speaking English, maternal age 18 years or older, and full-term singleton birth (37 weeks GA or older). Excluded were women with alcohol or other substance abuse (marijuana use was not excluded; see Supplement Material for details on prevalence of reported marijuana use and relation to primary outcome metrics). Anatomic MR images were reviewed by a neuroradiologist (J.S.S.) and pediatric neurologist (C.D.S.). Subjects were excluded from the current study if they had any evidence of brain injury. Additional exclusion criteria included pregnancy complications and known fetal abnormalities, including intrauterine growth restriction. Of the 385 participants who were scanned for eLABE, 262 were included in the current analyses. Subjects were excluded for the following reasons: no fMRI data collected ($n = 3$), no usable T2 for registration ($n = 28$), <37 weeks GA at birth ($n = 52$), brain injury ($n = 17$), required intubation or chest tube ($n = 4$), in the neonatal intensive care unit for >7 days ($n = 30$), and birthweight < 2,000 g ($n = 1$). There were 279 neonates who did not meet any of these exclusion criteria (note that some met multiple exclusion criteria). An additional 8 neonates were excluded because they did not have ≥10 min of usable fMRI data after motion censoring (see below), and 9 were excluded based on visible artifacts in functional connectivity data, resulting in 262 subjects in the current study.

In the eLABE dataset, maternal depression was assessed using the Edinburgh Postnatal Depression Scale (Cox et al. 1987) at each trimester and averaging over all available assessments. Total maternal perceived stress was measured with the Perceived Stress Scale (Cohen and Williamson 1988) at each trimester and averaging over all available assessments. SES was assessed with the area deprivation index (ADI) as determined by home address at the time of birth (Kind and Buckingham 2018). Demographics of the current sample are listed in Table 1 and zero-order relations among variables are listed in Supplementary Table 1.

Table 1. Sample characteristics.

Neonatal characteristics ($n = 262$)	n	Mean	SD
Sex			
Male	141		
Female	121		
Gestational age at birth in weeks		38.5	1.0
Postmenstrual age at scan in weeks		41.4	1.3
Birthweight in grams		3,272.6	489.5
Area deprivation index		68.0	24.9
Child's race			
African American	157		
White	98		
Chinese	2		
Other Pacific Islander	1		
Other	1		
Mixed African American/White	2		
Mixed Chinese/White	1		
Ethnicity			
Hispanic	6		
Non-Hispanic	256		
Neonatal fMRI characteristics	**n**	**Mean**	**SD**
Amount of fMRI data in minutes		16.6	4.4
Percent of frames retained		88.0	10.3
Maternal characteristics	**n**	**Mean**	**SD**
STAI trait anxiety		31.5	8.0
STAI state anxiety		28.1	7.7
Edinburgh Postnatal Depression scale		4.6	3.9
Perceived Stress scale		13.1	6.3

Child participants were from a study of attention-related disturbances in pediatric anxiety disorders conducted at Washington University of which details have previously been reported (Gilbert et al. 2020; Perino et al. 2021a, 2021b). The scanned sample included 61 children, average age 10.5 years (range 8.1–13.0). Thirty-one had an anxiety disorder (generalized anxiety disorder, social phobia, and separation anxiety), 29 had no psychiatric history, and 1 had prior history of adjustment disorder with anxious mood but no current psychiatric diagnosis. Exclusion criteria included current use of psychotropic medication, intellectual disability, autism, and learning disabilities.

Adult participants were derived from a sample of 120 adults (60 females; average age 25 years, range 19–32 years) that were collected at Washington University and have been previously extensively described (Power et al. 2011; Gordon et al. 2016). Exclusion criteria included a reported history of a psychiatric or neurological disorder.

fMRI data collection and acquisition parameters: neonates

After feeding, the infant was swaddled and positioned in a head-stabilizing vacuum fix wrap (Mathur et al. 2008). A nurse familiar with neonate transport and resuscitation was present at all MRI scans. Heart rate and blood oxygenation were measured continuously throughout all scans, and infants were monitored visually via video. Based on visual monitoring through a camera, infants slept through scans as indicated by eye closure and minimal movements. Imaging was performed without sedating medications using a Siemens 3T PRISMA scanner and 64-channel head coil. A T2-weighted image (sagittal, 208 slices, 0.8-mm isotropic resolution, echo time [TE] = 563 ms, tissue T2 = 160 ms, repetition time [TR] = 3,200 ms, or 4,500 ms) was collected. For the resting-state fMRI, functional imaging was performed using a BOLD gradient-recalled echo-planar multiband (MB) sequence (72 slices, 2.0-mm isotropic resolution, TE = 37 ms, TR = 800 ms, and MB factor = 8). Spin-echo field maps were obtained (at least 1 anterior–posterior and 1 posterior–anterior) during each session with the same parameters. We acquired between 2 and 9 fMRI BOLD scans, depending on how the infant tolerated the scan (mean 3.75 runs). Scans were collected in both the anterior-to-posterior (AP) and posterior-to-anterior (PA) direction; a typical scan session included 2 AP runs and 2 PA runs. AP and PA scans were concatenated following fMRI preprocessing but prior to computation of functional connectivity values (i.e. immediately prior to computing correlations). The scans were 420 frames, which is 5.6 min in length. Framewise integrated real-time MRI monitoring (FIRMM) (Dosenbach et al. 2017) was used during scanning to monitor real-time participant movement.

fMRI data collection and acquisition parameters: children

Imaging was performed on a Siemens PRISMA 3T MRI scanner with a 32-channel head coil. Structural images included a T1-weighted image (sagittal, 208 slices, 0.8-mm isotropic resolution, TE = 2.22 ms, TR = 2,400 ms, TI = 1,000 ms, and flip angle = 8°), and a T2-weighted image (sagittal, 208 slices, 0.8-mm isotropic resolution, TE = 563 ms, tissue T2 = 160 ms, and TR = 3,200 ms). Functional imaging was performed, including 4 resting-state runs (420 frames each), using a blood-oxygen-level dependent multi-band echo-planar sequence (TR = 720 ms, TE = 33 ms, flip angle = 52°, 2.4-mm isotropic resolution, MB factor = 7). Two spin-echo field maps were obtained (1 AP and 1 PA) during each session with the same parameters. FIRMM (Dosenbach et al. 2017) was used during scanning to monitor real-time participant movement. Sessions were terminated if/when participants showed an inability to stay still during the scan, as determined by experienced clinical research assistants, which resulted in 10 children being excluded for either excessive head motion or because they could not tolerate scanning, leaving a final neuroimaging sample of 61 children.

fMRI data collection and acquisition parameters: adults

MRI data in the adult group-average dataset were obtained with a Siemens MAGNETOM Trio Tim 3.0T Scanner (Erlangen, Germany) and a Siemens 12 channel

Head Matrix Coil. Structural images obtained included a T1-weighted sagittal MP-RAGE (magnetization-prepared rapid acquisition gradient echo; TE = 3.08 ms, TR(partition) = 2.4 s, TI = 1,000 ms, flip angle = 8°, and 176 slices with 1 isotropic resolution), as well as a T2-weighted turbo spin-echo structural image (TE = 84 ms, TR = 6.8 s, 32 slices with 1 × 1 × 4-mm voxels). Functional imaging was performed using a BOLD contrast sensitive gradient echo echo-planar sequence (TR = 2.5 s, TE = 27 ms, flip angle = 90°, 4-mm isotropic resolution, and 32 axial slices). Across subjects, the number of collected volumes ranged from 184 to 729 (mean = 336 frames and 14.0 min).

fMRI preprocessing

fMRI preprocessing was done with minor variations in each dataset in order to optimize data quality metrics (e.g. registration errors and signal-to-noise, SNR) for each dataset. Because of large differences in head size, different locations and causes of artifacts inherent to imaging different ages (Kaplan et al. 2022), different magnetic properties of tissues at different ages (Thornton et al. 1999; Smyser and Neil 2015; Liu et al. 2016; Goksan et al. 2017; Neil and Smyser 2018), and the size of voxels relative to the thickness of gray matter, we chose to optimize each processing pipeline specific to each dataset rather than choose a "one-size-fits-all" approach. In our opinion, using a one-size-fits-all approach would compound the inherent methodological problems because measurements of BOLD activity would be suboptimal (noisier) in one of the groups. In the text below, methods were identical across the 3 datasets unless otherwise noted. Flowcharts of the processing pipelines are also provided in Supplementary Figs. 1 and 2 and facilitate comparisons across age groups.

fMRI preprocessing included correction of intensity differences attributable to interleaved acquisition, linear realignment within and across runs to compensate for rigid body motion, bias field correction (neonates and children only), intensity normalization of each run to a whole-brain mode value of 1,000, readout distortion correction (neonates and children only), and linear registration of BOLD images to the adult Talairach isotropic atlas (Talairach and Tournoux 1988). Neonates were registered: BOLD → individual T2 → cohort-specific T2 atlas → 711-2N Talairach atlas. The cohort-specific T2 atlas used as an intermediate step in the registration was created from a subset of 50 neonates from this study. The children and adults were registered: BOLD → individual T2 → individual T1 → 711-2B Talairach atlas. Linear registrations were performed in a single step (Smith et al. 2004). Field (readout) distortion correction was performed in neonates and children only, using the FSL TOPUP toolbox (http://fsl.fmrib.ox.ac.uk/fsl/fslwiki/TOPUP).

The volumetric registrations of BOLD data described previously for all 3 datasets were linear, included 12 degrees of freedom, had no nonlinear components, and used in-house software (ftp://imaging.wustl.edu/pub/raichlab/4dfp_tools/). The final product of this preprocessing was the subject's own BOLD data linearly registered to adult Talairach space. In subsequent steps, described below, these volumetric BOLD data were mapped to the subject's own surface. Each subject's surface was created from an anatomical image (T1 for children and adults, T2 for neonates) that had also been linearly transformed to adult Talairach space; thus the 3D coordinate systems for the preprocessed volumetric BOLD data and the anatomical surface were the same. As described below, subject-specific surfaces are aligned to a common surface space (fsLR_32k), a process that is inherently nonlinear. All registrations (volumetric and surface) were visually inspected to ensure accuracy.

Following the initial preprocessing, the resting-state BOLD timeseries underwent functional connectivity processing (Power et al. 2014; Gordon et al. 2016). In the children and adults, functional connectivity (fc) processing was done in volume-space (note, however, that for children and adults, functional connectivity processed data were mapped to subject-specific surfaces prior to further functional connectivity analyses and subject averaging, so the child and adult analyses are surface-aligned). In the neonates, data were first mapped to the surface (see below), minimally smoothed with a small geodesic 2D Gaussian kernel (σ = 1 mm), and functional connectivity processing was done in surface space. First, temporal masks were created, which censored high-motion frames based on study-specific protocols described below. Then the censored frames were ignored as the data were functional connectivity processed with the following steps: (i) demean and detrend within run, (ii) multiple regression with nuisance timeseries including white matter, ventricles, and whole brain, as well as 24 parameters derived from head motion (x, y, z, roll, pitch, yaw on the current and previous frames; and the squares of these 12 parameters). For neonates, the whole-brain signal was the average gray matter signal; in the other datasets the whole-brain signal was from a whole-brain mask. The neonates also included an additional extra-axial space regressor. Finally, retained data were interpolated into censored timepoints to allow band-pass filtering (0.005 Hz < f < 0.1 Hz for neonates; 0.009 Hz < f < 0.08 for children and adults).

Neonatal fMRI data were censored at framewise displacement (FD) > 0.25 mm, with the additional restriction that only epochs of at least 3 consecutive frames with FD < 0.25 mm were included. To be included in the study, a minimum of 10 min of data were required. In children, a first-order low-pass Butterworth filter (cutoff 0.1 Hz) was applied to each of the 6 head realignment parameters, which were then summed to create a filtered FD trace (Fair et al. 2020). Frames with filtered FD > 0.08 mm were censored, and functional runs with fewer than 130 frames were excluded. Only the 61 subjects with at least 670 remaining frames (8.04 min) were included in further analyses. For adults, volumes with FD > 0.2 mm or DVARS > 5.36 were censored; a minimum of 6-min total data were required.

In each dataset, MCRIB (neonates; Alexander et al. 2017; Adamson et al. 2020) or Freesurfer (children and adults; Dale et al. 1999; Fischl et al. 1999) was used to generate surfaces for each subject. For surface-based analyses, the volumetric fMRI data (in children and adults, after fc-processing; in neonates, after standard pre-processing but before fc-processing) were mapped to subject-specific surfaces using established procedures adapted from the Human Connectome Project as implemented in Connectome Workbench 1.2.3 (Marcus et al. 2011, 2013). fMRI data were aligned across subjects into the "fs_LR32k" surface space using spherical registration (Glasser et al. 2013). Timecourses for surface data were smoothed with geodesic 2D Gaussian kernels after fc-processing ($\sigma = 2.25$ mm for neonates and $\sigma = 2.55$ mm for children and adults). rs–fc was computed as the Fisher z-transformed Pearson correlation between timecourses from pairs of surface vertices or surface parcels, as detailed below.

In addition to these surface-based analyses, the neonatal dataset was also analyzed in volume space. In this case, the volumetric preprocessed data (as described previously) were spatially smoothed in volume space with a 3-mm FWHM Gaussian kernel and functional connectivity processing was completed in volume space. These data were then mapped to a group-average neonatal surface in fs-LR32k space. Because the data were not each mapped to their own individual surface, there was no surface-based alignment. Functional connectivity was then computed in the group-average surface-space as the Fisher z-transformed Pearson correlation between timecourses from pairs of vertices.

Functional connectivity matrices

Initial analyses computed parcelwise functional connectomes from each individual in each dataset. Resting-state functional connectivity was computed in each subject between pairs of parcels from (Gordon et al. 2016), a validated set of surface parcels that were constructed on the basis of the adult dataset that was used in the current study. Pairwise functional connectivity among parcels defined individual parcelwise functional connectivity matrices. Group-average parcelwise functional connectivity matrices were also created for each of the 3 datasets (neonatal, child, and adult), and similarity among the 3 datasets was computed as the correlations between pairs of group-average parcelwise functional connectivity matrices.

To visualize seed-based functional connectivity of posterior clusters for each adult-defined network, we defined seeds based on the centers of network clusters (contiguous portions of cortex from the same functional network) from (Power et al. 2011; see Supplementary Fig. 5). Functional connectivity was computed for each seed to every other vertex for each individual, and then these network-specific seed-maps were averaged across each of the 3 datasets. To compare pairs of datasets (e.g. the DMN seed maps in neonates versus adults), spatial Pearson correlations were computed across the 2 group-average seed maps. To characterize the overall functional connectivity strength for each individual's seed map, the root sum of squares deviation from zero (RSSE) was computed by taking the square root of the sum of squares for all values in a seed map. The RSSE was then compared between groups for a specific seed map (e.g. comparing the overall functional connectivity strength of the DMN seed-map in neonates versus adults) with 2-sample *t*-tests. Relations between RSSE and neonatal cortical thickness are provided in the Supplementary Results.

A next set of analyses compared the topography of positive and negative functional connectivity for each seed map. Seed maps were first masked to only include vertices in the same hemisphere and at least 30 mm away from the seed. We then created binarized maps for the top 20% of positive functional connections and the top 20% of negative functional connections, by magnitude, for each group-average seed map (additional thresholds are in Supplementary Table 2). The Dice coefficient was then computed between pairs of group-average binarized maps (e.g. the overlap in negative functional connections for the DMN seed map in neonates versus adults). To compare whether the overlap in positive functional connectivity was significantly different than the overlap in negative functional connectivity for a specific seed map, we permuted the identity of subjects within each group 10,000 times and computed the difference in overlap for each permutation. For example, for comparing neonates versus adults, we permuted whether an individual was an adult versus neonate, maintaining the sample sizes from the original datasets. The *P*-value was determined by comparing the true difference in overlap for positive versus negative functional connections with the values from the permutations.

Long- and short-range selectivity

For the long-range selectivity analyses, we computed functional connectivity among adult-derived network clusters from (Power et al. 2011). For the analyses in the main text, functional connectivity between activity from a posterior network cluster from 1 of 5 networks (DMN, DAN, FPN, cingulo-opercular network [CON], and ventral attention network [VAN]) was computed with activity from an anterior network cluster for each of the 5 networks. We tested for selectivity for each dataset (neonate, child, and adult) with a series of paired *t*-tests in which functional connectivity to same-networks (e.g. posterior DMN to anterior DMN) was compared with functional connectivity between-networks (e.g. posterior DMN to anterior DAN). We next defined a single selectivity value for each posterior network cluster as the difference in functional connectivity to the anterior network cluster from the same network minus the average functional connectivity to the other 4 anterior network clusters. These selectivity values were compared across datasets using 2-sample *t*-tests. A parallel set

of analyses examined selectivity of anterior network clusters for posterior network clusters.

To compare between-network functional connectivity within the frontal lobe among the 3 datasets, we computed the average functional connectivity of each network cluster in the frontal lobe to clusters for other networks. The networks included were the DMN, FPN, DAN, VAN, and CON. We used a series of 2-sample *t*-tests to compare this average functional connectivity value across the 3 groups. A parallel analysis was computed for the posterior cortex. Relations of long- and short-range selectivity to neonatal cortical thickness are provided in the Supplementary Results.

Neonatal functional brain networks

We used the community detection algorithm Infomap (Rosvall and Bergstrom 2008; Power et al. 2011) to empirically derive functional brain network assignments in neonates. A first set of analyses were performed on the vertexwise functional connectivity data. The group-average vertexwise neonatal functional connectivity matrix was first masked to set any functional connections <49 mm in adult Talairach atlas space to zero (~30 mm in native neonatal space), so that network solutions were not driven by local spatial smoothing. Next, the top X% of positive functional connections (X ranging from 0.25 to 10 in separate analyses) were set to one and all other functional connections were set to zero. This thresholded, binarized functional connectivity matrix was then subjected to Infomap. Colors at each edge density were manually selected to maintain consistency across edge densities.

In a second analysis, we ran Infomap on contiguous network pieces derived from the empirical network solution described above at edge density 1.25%. In this case, we first zeroed out any functional connections between pieces in which any portion of the pieces were within 30 mm of each other. Next, Infomap was run as described previously.

Maturity index in relation to registration technique and data quantity

A maturity index (MI) was computed for each individual neonate as the correlation between the individual's vertexwise functional connectivity matrix and the adult group-average vertexwise matrix. The MI is expected to index apparent neonatal brain maturity because it directly measures similarity to adult data. We first tested whether MI varied depending on whether the data were aligned across subjects in surface-space versus exclusively volume-space. For this analysis, the MI values of the vertexwise functional connectivity matrices for surface- versus volume-based registration were compared using a paired *t*-test. We next tested the degree to which per-participant data quantity was related to apparent neonatal maturity. For this analysis, we computed the correlation between retained data and MI across subjects. Additional analyses computed correlations between MI and socio-demographic variables (Supplementary Table 1). Next, regressions were performed in which MI was related to data quantity while controlling for socio-demographic variables that were significantly related to MI. Finally, for subjects with at least 20 min of low-motion data ($n = 71$), we also computed the MI for the first 10 and for the first 20 min of data collected, and then we performed a paired *t*-test to examine within-subject relations between data quantity and MI.

Because of the large effect sizes in most of the group comparisons and the large number of subjects, most of the statistical tests described in the results were highly statistically significant. For ease of reporting, we use the notation "$P << 0.001$" for results in which $P < 1 \times 10^{-5}$. We report uncorrected *P*-values but note that all primary analyses survive Bonferroni correction.

Results

Whole-brain and seed-based neonatal functional connectivity

Sample characteristics of the $n = 262$ neonates are listed in Table 1 and zero-order relations among demographic variables are provided in Supplementary Table 1. Resting-state functional connectivity data from each dataset (neonate, child, and adult) were scaled and aligned to a common surface space with vertex-to-vertex correspondence (Van Essen et al. 2012) to facilitate comparisons across groups. The whole-brain functional connectivity pattern of neonates was moderately correlated with both children ($r = 0.65$, $P << 0.001$) and adults ($r = 0.64$, $P << 0.001$), whereas adult and child whole-brain functional connectivity patterns were highly correlated with each other ($r = 0.91$, $P << 0.001$). Group-average whole-brain functional connectivity matrices from each dataset are depicted in Supplementary Fig. 3.

We visually compared whole-brain functional connectivity patterns of individual vertices across neonates, children, and adults (Fig. 1 and Supplementary Fig. 4). Seed vertices were the centers of brain regions from adult-defined networks ("network chunks," see Supplementary Fig. 5). For the adults, these seed maps generated typical patterns of positive and negative correlations associated with established functional brain networks. Seed-maps for children largely resembled maps for adults (*r* values from 0.86 to 0.95, all $P << 0.001$). However, the similarity of seed-maps between neonates and adults differed by functional network, with most correlations around 0.75 (FPN: 0.75; DAN: 0.74; Ventral attention network, VAN: 0.73; Salience Network, SN: 0.76; and DMN: 0.73); a lower correlation for the cingulo-opercular network (CON) seed (0.56); and relatively high correlations for the auditory (AN, 0.89), visual (VN, 0.83), and somatomotor-hand (SMN-h, 0.87) seeds (all $P << 0.001$). Similarity of seed-maps between neonates and children ranged between 0.58 and 0.84 and largely resembled neonate/adult comparisons.

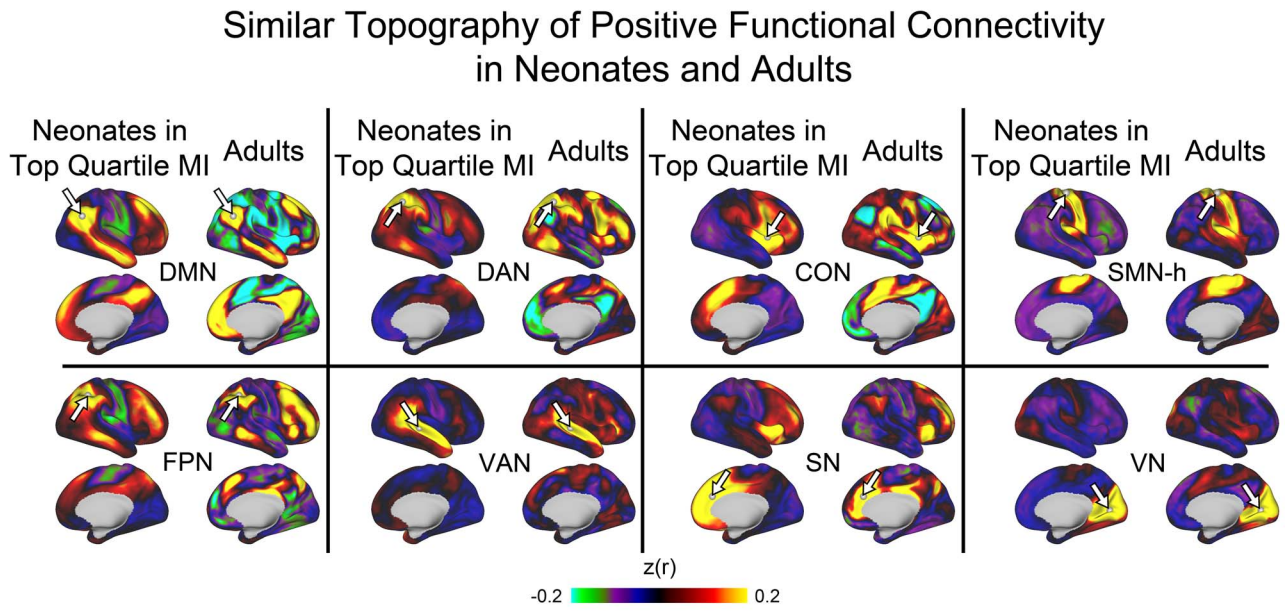

Fig. 1. Seed-based functional connectivity patterns of posterior seeds (white arrows) in neonates and adults. Seeds are derived from centers of network clusters based on adult assignments (Power et al. 2011). Note that the topography of positive connectivity is similar across the datasets, though the magnitude is weaker in neonates. This figure depicts neonates in the top quartile of MI, which indexes both brain maturity and data quality (see Results). Seed maps for the full neonatal dataset, in children, and in additional functional networks are in Supplementary Fig. 4. DMN: default mode network; DAN: dorsal attention network; CON: cingulo-opercular network; SMN-h: hand somatomotor network; FPN: fronto-parietal network; VAN: ventral attention network; SN: salience network; VN: visual network.

The data above indicate that neonatal functional connectivity patterns of individual seeds are moderately to highly correlated with adult and child patterns. Additional analyses revealed, however, that neonatal seed maps differed in several aspects from adult seed maps. First, the magnitudes of functional connectivity values (including both positive and negative functional connectivity) were generally lower in neonates compared with adults. As detailed in the Supplementary Results, the root sum of squares deviation from zero (RSSE) was lower for neonates compared with adults (all $P < 0.001$) for seeds from the DMN, FPN, DAN, VAN, SN, CON, and VN; but not the SMN-h. A second difference between neonates and adults was the topography of negative correlations. Based on visual inspection (Fig. 1), although the locations of positive functional connectivity values were similar in neonates and adults, the locations of negative functional connectivity values appeared different in neonates and adults. As detailed in the Supplementary Results, quantitative tests supported this observation, as neonatal-adult overlap of positive functional connectivity was significantly greater than the neonatal-adult overlap for negative functional connectivity for the DMN, FPN, DAN, CON, and SMN (but not the VAN or SN) seeds. Comparisons for neonates versus children and for children versus adults are provided in the Supplementary Results.

Network-selectivity of long- and short-range neonatal functional connectivity

The analyses above indicate that, overall, the positive functional connectivity patterns of individual seeds in the neonate are similar to older children and adults. However, the analyses above do not specifically test whether seeds have higher functional connectivity to spatially distant brain regions from the same versus different adult-defined functional networks. Thus, we next tested for network selectivity of long-range functional connections in the neonates.

Results indicated that for DMN, FPN, and DAN posterior network clusters, functional connectivity was highest with the corresponding adult-defined anterior cluster region relative to clusters from other networks (see Fig. 2A and Supplementary Fig. 6, all pairwise paired t-tests $P < 0.001$). For example, in neonates, the posterior FPN cluster had highest functional connectivity to the anterior FPN cluster compared with its functional connectivity to anterior clusters from the DMN, DAN, CON, or VAN. The same pattern of results was obtained when examining selectivity of anterior network cluster seeds for posterior network clusters as delineated in Supplementary Fig. 7.

We next compared the degree of this long-range selectivity across age groups. Selectivity of long-range functional connections from clusters in the posterior DMN, FPN, and DAN to anterior clusters from the same network was lower in neonates relative to adults and children (see Fig. 2A and Supplementary Fig. 6, all P values $<< 0.001$). This result remained consistent when functional connectomes from all 3 datasets were rescaled to have the same mean and variance (all P values $<< 0.001$) and when examining selectivity of long-range functional connections from anterior clusters to posterior clusters (Supplementary Fig. 7). When

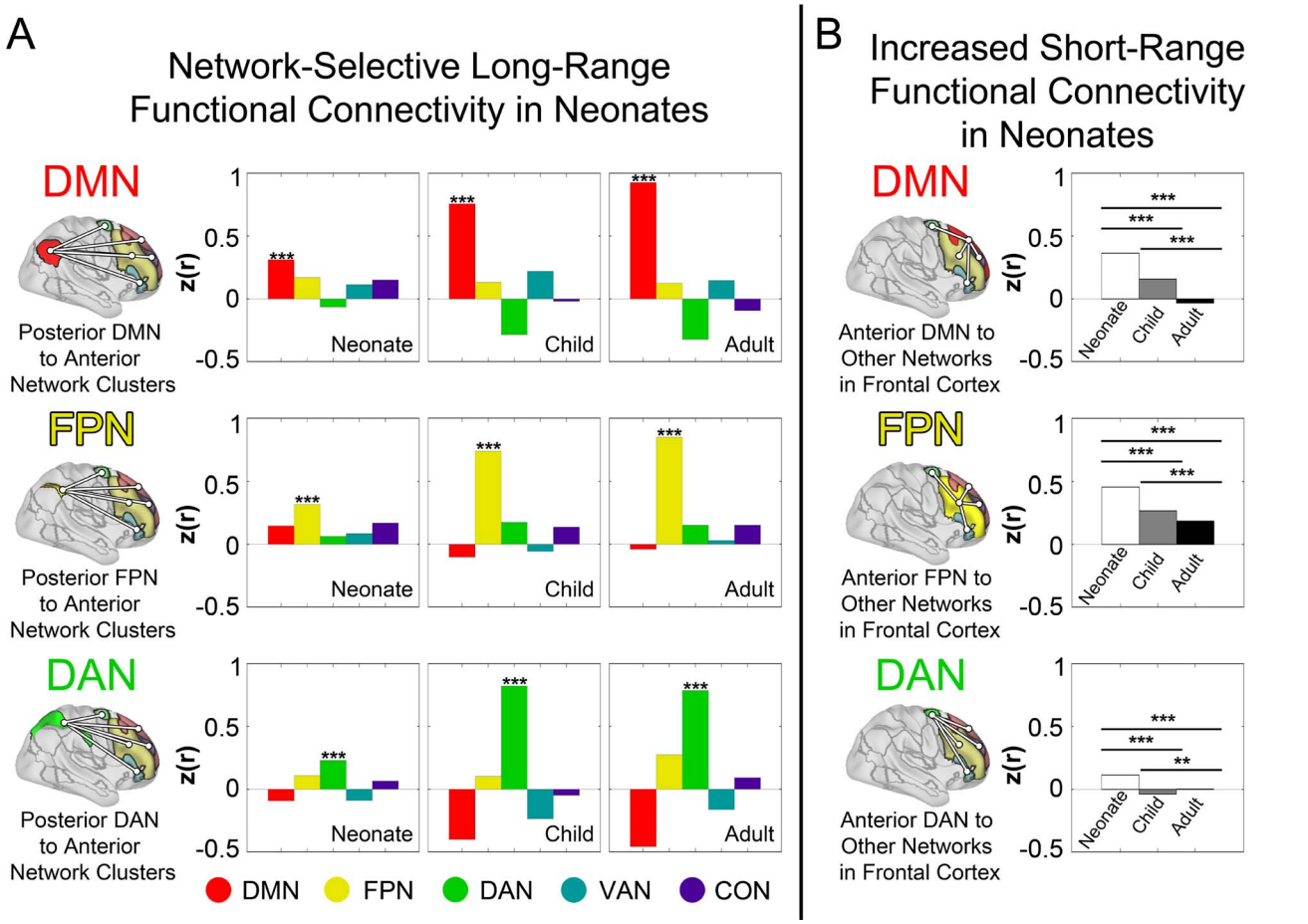

Fig. 2. Neonates have present but reduced network-specificity of long-range functional connectivity and increased short-range functional connectivity relative to older children and adults. **Panel A** provides bar graphs plotting PA functional connectivity at 3 different ages. For each network, functional connectivity is plotted between a single posterior network cluster and 5 different anterior network clusters from 5 different networks. Network assignments are based on work in adults (Power et al. 2011). For the DMN, FPN, and DAN posterior seeds, functional connectivity was highest to the anterior cluster corresponding to the same network at all 3 ages, including neonates (astericks indicate bars with significantly higher values relative to all other bars in pairwise comparisons). Thus, there is network-specific selectivity of long-range functional connectivity in the neonatal brain. Note, however, that the selectivity for same- versus different- network functional connectivity is not as great in neonates as in the other ages. **Panel B** illustrates the average functional connectivity of frontal lobe network clusters to 4 other clusters (DMN, FPN, DAN, CON, and VAN minus whichever network is the seed) in the frontal lobe, each from different networks. Note that the average (short-range) functional connectivity to other functional networks is highest in neonates, intermediate in children, and lowest in adults. *** ($P << 0.001$); ** ($P = 0.01$).

comparing adults and children, adults had higher long-range selectivity for DMN ($P << 0.001$) and FPN ($P = 0.03$) seeds, whereas children had higher long-range selectivity for the DAN seed ($P = 0.008$).

We next compared short-range functional connectivity across neonates, children, and adults. First, we measured between-network functional connectivity within the frontal lobe (Fig. 2B and Supplementary Fig. 8). The average functional connectivity of each network cluster in the frontal lobe to clusters for other networks in the frontal lobe was highest in neonates (indicating lower network specificity of functional connectivity), intermediate in children, and lowest in adults (all pairwise $P < 0.001$). The same pattern of results was obtained when examining functional connectivity within the posterior cortex (Supplementary Fig. 9).

Empirically defined neonatal functional networks

We next empirically defined neonatal functional brain networks and explored the extent to which the features described above (present but decreased selectivity of long-range functional connections; increased short-range functional connectivity) impacted results of different network-detection algorithms. We first used a standard implementation of the community detection algorithm Infomap to empirically derive functional brain networks in neonates over a range of edge densities (Fig. 3). This approach permits characterization of network organization when considering relatively weak functional connections ("dense edge densities") versus when considering only the strongest functional connections ("sparse edge densities"). At dense edge

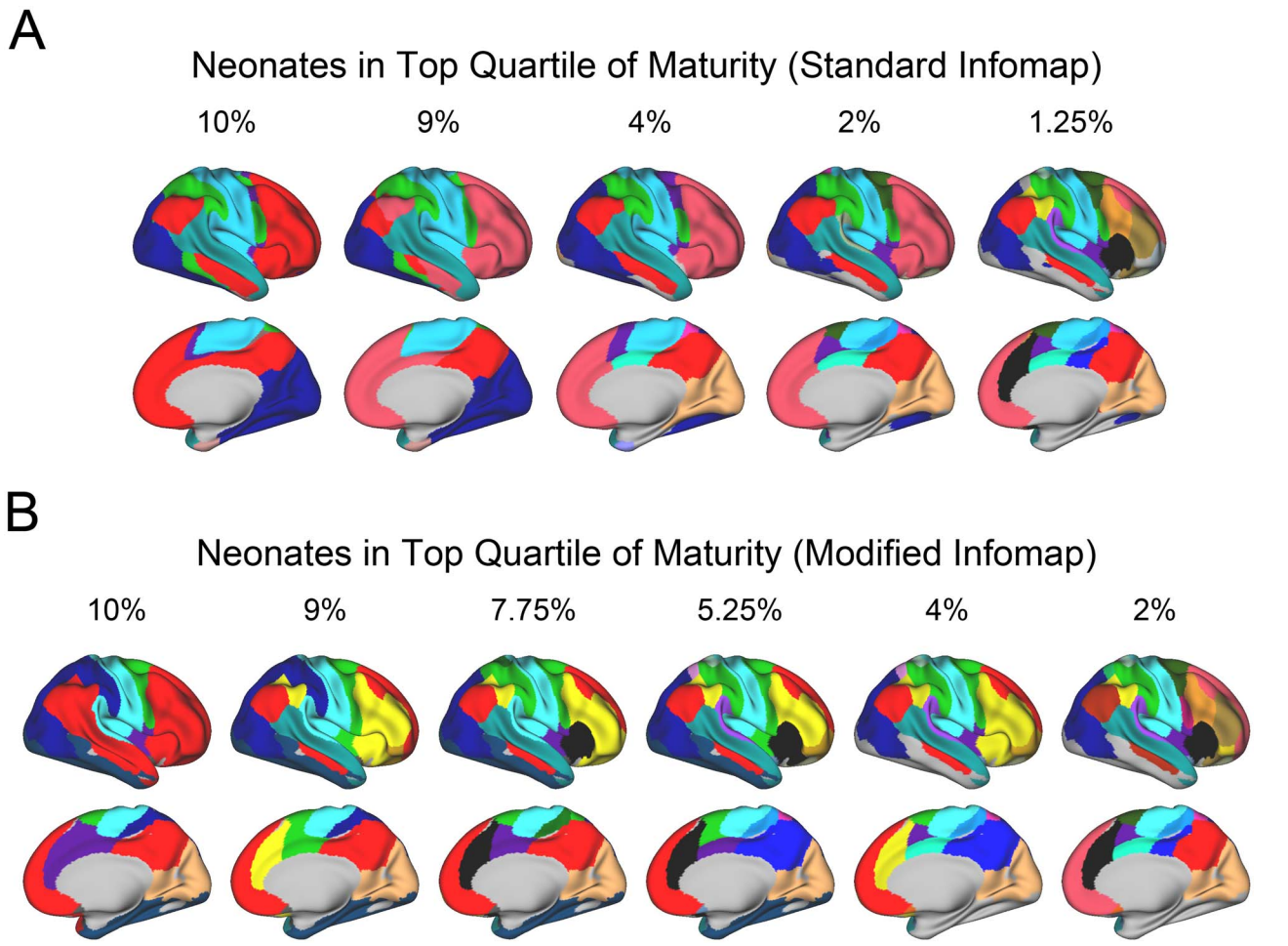

Fig. 3. A latent adult-like functional network organization exists in the neonatal brain. **Panel A** depicts empirically derived functional brain networks using a standard vertexwise community detection algorithm (Infomap) across a range of edge densities. Numbers above each brain indicate the top X% of functional connections used the derive the functional network solution. Note that as progressively weaker functional connections are considered (e.g. at dense edge densities such as 9–10%), some distributed networks emerge (in red and green). **Panel B** depicts functional network identities derived using a modified Infomap algorithm that favors long-range functional connections, when restricting analyses to neonates in the top quartile of MI. Note that when long-range functional connections are favored, many adult-like patterns emerge.

densities (10%), a 6-network solution emerged including networks that resembled the adult VN (dark blue), SMN (light blue), posterior VAN (teal), and anterior CON (purple). In addition, there were 2 networks (green and red) with regions distributed across the brain. The green network resembled the DAN in adults and the red network included most of the frontal lobe and resembles the combined DMN and FPN in adults. The DMN and FPN did not segregate at any edge density using this standard algorithm. For network solutions at sparser edge densities, the networks described above break into progressively smaller pieces.

To examine for latent adult-like organization that might not be evident when using the standard algorithm, we next used an algorithm that employed neonatal-defined regions and emphasized long-range functional connections over short-range functional connections (see Methods). By using this procedure, we derived a network solution resembling adult-like assignments (Fig. 3B). More specifically, segregated networks with some elements similar to the adult-defined DMN, DAN, FPN, CON, and SN could be identified in the neonates. The DMN and FPN were segregated in this scheme, indicating that some differentiation between these functional networks is present during the neonatal period. The functional connectivity matrices based on these network assignments exhibited a typical block structure (Supplementary Fig. 10). It is important to note that the algorithm in no way imposed an adult-like structure (i.e. there were no adult "priors"). Were it not for selectivity in the long-range functional connections described above, another more arbitrary network solution would have emerged. Taken together with the results above, these results indicate that there is a latent adult-like organization of neonatal functional connections; but that this organization is obscured by high short-range functional connectivity and decreased long-range selectivity.

Apparent maturity of neonatal functional networks depends on registration and data quantity

Results from the current study suggest that the neonatal brain has adult-like organizational features. We next examined the extent to which 2 specific design elements of the current study, surface-based registration and high per-subject data quantity (10–30 min after frame censoring), contributed to the measured maturity of the neonatal brain. For each neonate, we computed a MI, as the similarity (correlation) in whole-brain functional connectivity between that neonate and an adult average. The MI is expected to index apparent neonatal brain maturity because it directly measures similarity to adult data. Consistent with our hypothesis, MI was higher when using surface-based registration compared with using exclusively volume-based registration (Fig. 4A; 0.45 versus 0.42, $t(261) = 38.5$, $P << 0.001$). Out of the 262 neonates, 259 had a higher MI value with surface-based compared with volume-based registration. Second, as predicted, MI was strongly correlated with the amount of available low-motion fMRI data ($r = 0.61$, $P << 0.001$), with no clear plateau in this relation even with 30 min of data (Fig. 4B). After controlling for the amount of retained data, there was a significant relation between neonatal MI and postmenstrual age (PMA) at scan (partial $r = 0.30$, $P < 0.001$, Fig. 4C), consistent with the MI also indexing maturity. We also computed the MI in the subset of neonates with at least 20 min of low-motion data ($n = 71$), restricting the MI calculation to the first 10 or 20 min of imaging data collected. Using this within-subject approach, MI was significantly higher with 20 versus 10 min of data (0.48 vs. 0.42, $t = 26.1$, $P << 0.001$). Thus, there was support for the hypothesis that apparent functional brain maturity (as measured with MI) is dependent on data quantity. Supplementary Fig. 3B depicts functional connectivity matrices from individual neonates across a range of MI values.

Discussion

The goals of this study were to characterize the functional network organization of the neonatal brain and to test whether long-range functional connections in neonates exhibit network-selectivity similar to school-age children and adults. Results indicated that long-range selective functional connectivity is identifiable in neonates for several adult-defined networks, including the DMN, DAN, and FPN. This selectivity is weaker relative to school-age children and adults, and neonates additionally have stronger local functional connectivity compared with older samples. This weak long-range selectivity combined with increased local functional connectivity results in a standard community detection algorithm primarily segregating the neonatal brain into networks consisting of isolated anatomical pieces of cortex. However, when the algorithm is tuned to favor long-range functional connections, an adult-like pattern of functional brain networks emerges. Functional connectivity overall is weaker in neonates relative to older samples, and the pattern of positive functional connectivity is more similar between neonates and adults compared with the pattern of negative functional connectivity. Finally, neonatal functional brain networks appear more adult-like when using surface-based registration as opposed to volume-based registration; and when using greater amounts of imaging data per participant.

This study reveals that long-range functional connections characteristic of adult functional brain networks, including the DMN, DAN, and FPN, also exhibit network-selectivity near the time of birth. In other words, contiguous portions of cortex in the neonate that share a common adult-defined network assignment show greater functional connectivity to spatially distant cortex from the same adult-defined network than to spatially distant cortex from different adult-defined networks. These results discount an alternative developmental model in which long-range functional connections are nonspecific near the time of birth and selectivity emerges over the first years of life. These results extend prior work that has reported functional connectivity between anterior and posterior regions that become the DMN in adults (Doria et al. 2010; Smyser et al. 2010, 2016; Keunen et al. 2017; Molloy and Saygin 2022); the current study demonstrates that this long-range functional connectivity is network-selective and also provides evidence for long-range selectivity of functional connections in the nascent DAN and FPN.

We demonstrate that selective, network-specific, long-range functional connections for the DMN, DAN, and FPN are present near the time of birth. The detection of purely localized versus segregated functional networks when using whole-brain network-detection algorithms depends on the algorithm used and is a consequence of neonatal functional connectivity properties. Because local functional connectivity is higher in neonates, and the degree of long-range selectivity is modest, a standard algorithm detects localized networks because of the high local functional connectivity. An algorithm tuned to emphasize long-range functional connectivity, in contrast, derives more adult-like networks because selective long-range functional connections are present near birth but weaker compared with older samples. These observations reconcile seemingly inconsistent findings from prior studies, some of which report anterior–posterior segregated neonatal networks, whereas others characterize neonatal functional networks as consisting primarily of bilateral segregated anatomical pieces of cortex (Fransson et al. 2007, 2009; Gao et al. 2009; Doria et al. 2010; Smyser et al. 2010; Gao et al. 2013; De Asis-Cruz et al. 2015; Gao et al. 2015; van den Heuvel et al. 2015; Gao et al. 2016; Smyser et al. 2016; Keunen et al. 2017). That is, prior work using nonlinear methods such as thresholding of seed-based functional connectivity maps or ICA-based network-detection algorithms likely highlighted the high

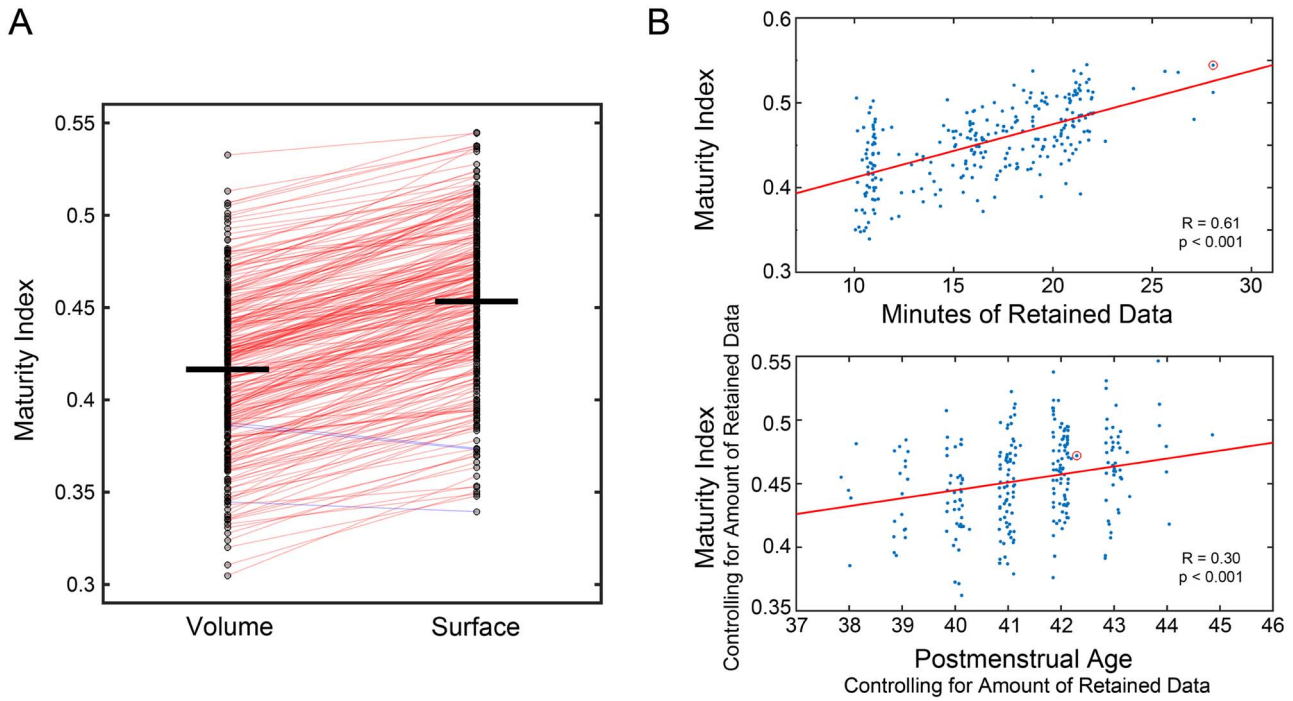

Fig. 4. Neonatal functional brain networks appear more adult-like when using surface-based alignment and as per-participant data quantity increases. **Panel A** illustrates the apparent maturity of neonatal functional connectivity depending on whether surface-based or volume-based alignment strategies were used. Lines connect MI values for individual neonates using volume-based versus surface-based alignment. Out of 262 neonates, the MI value was higher in 259 with surface-based registration (red lines); just 3 had higher MI values with volume-based registration (blue lines). The top section of **Panel B** provides a scatterplot of the significant relation between the MI (computed in surface-space) and amount of retained imaging data in the neonatal dataset. The red circle indicates a participant who was an outlier for minutes of retained data (42 min), and so their value was Winsorized (to 28 min). The bottom section demonstrates the significant relation between PMA at scan and MI, when accounting for amount of retained data.

magnitude short-range neonatal functional connections rather than the weaker long-range functional connections.

The current study is consistent with a model in which basic overall functional brain network organization, including selective long-range functional connections of the DMN, FPN, and DAN, are established in-utero (Turk et al. 2019; Thomason 2020) rather than over the first years of life. These results highlight the role of maternal-placental-fetal biology in establishing the foundational functional network architecture of the human brain and underscore the importance of understanding how maternal factors such as health, nutrition, and stress impact in-utero brain development (Entringer et al. 2015; Norr et al. 2021; Thomason et al. 2021; van den Heuvel et al. 2021). This basic organization may be flexibly honed over the first few years of life through decreases in short-range functional connectivity and increases in the selectivity of long-range functional connections (Gao et al. 2011; Cao et al. 2017; Shi et al. 2017) in order to develop experience-dependent topographies, permitting the environment to influence the more fine-grained details of functional connectivity. Although the specific structural correlates of this refinement in functional connectivity are not known, the first 2 years of life are a period of increasing myelination, axonal pruning, synaptogenesis, and synaptic pruning (Brody et al. 1987; Stiles and Jernigan 2010; Tau and Peterson 2010; Collin and van den Heuvel 2013; Keunen et al. 2017; Neil and Smyser 2018). The presence of emerging adult-like networks is also consistent with prior work indicating that spatially separated brain regions that process specific types of information (i.e. language and faces) are selectively functionally connected to each other in neonates (Kamps et al. 2020; Li et al. 2020) as they are in adults.

The current study also highlighted that one of the most striking differences between the neonatal and adult functional connectomes is the topography of negative functional connectivity, which exhibited greater age-related differences compared with the topography of positive functional connectivity. This observation is consistent with prior work arguing that negative functional connectivity between the DMN and DAN, the 2 networks with the strongest negative correlations, do not have significant negative correlations until the first year or two of life (Gao et al. 2013, 2015). Although the nature of negative correlations is incompletely understood, they are generally viewed as reflecting inhibition (Greicius et al. 2003; Fox et al. 2005). An important direction for future work is to clarify when negative correlations become more adult-like and how the maturation of negative correlations corresponds to developmental changes in information processing.

One prospect is that estimates of the maturity of the neonatal brain will continue to increase with advances

in data acquisition and processing. The decreased apparent long-range and short-range selectivity measured in neonates relative to older samples likely represents a combination of biological differences and methodological challenges that effectively blur the location of neonatal functional areas at the group-level. Further work is needed to continue to elucidate to what extent measured differences are related to biology versus methodological challenges. The improvement in apparent maturity from volume-based to surface-based alignment suggests it may be more difficult to align homologous functional brain areas across neonates. This assertion is supported by recent work revealing heterogeneity in the layout of functional networks across neonates (Molloy and Saygin 2022). Importantly, the effect of mis-aligning subjects and then averaging data across heterogeneous subjects would result in exactly the pattern of functional connectivity noted in neonates: higher apparent local functional connectivity and less selectivity of long-distance functional connectivity. Thus, methods that further account for heterogeneity may also result in additional increases in the apparent maturity of the neonatal brain. "Precision neuroimaging" is an approach in which large amounts (i.e. hours) of data are collected in individual participants over multiple days, significantly improving the reliability of measured signals (Laumann et al. 2015; Gordon et al. 2017; Sylvester et al. 2020). Analyses are performed within-subject and do not involve group-averaging. Such precision neuroimaging techniques could test whether functional networks appear more immature in group-average datasets because of averaging across heterogenous neonates. In addition, the increase in apparent maturity of the neonatal brain with increasing amounts of data suggests that lower SNR may make it more difficult to detect adult-like functional networks in neonates. One possibility that could be tested in the future is that techniques that increase SNR, including multi-echo sequences (Posse et al. 1999; Lynch et al. 2020), infant-specific head coils, and precision neuroimaging, may uncover further increases in the apparent maturity of the neonatal brain. Because neonatal functional connectivity appeared progressively more adult-like with increasing amounts of data, with no plateau in this relation even with 30 min of data, we also highlight the importance for future work to consider extended fMRI data acquisitions.

The current study should be viewed in light of its limitations. As noted throughout, comparisons across neonates, children, and adults are complicated by inherent methodological differences. These differences are unavoidable due to differences in head size (especially differences in the ratio of gray matter thickness to voxel size), differences in magnetic properties of tissues, and different sources of noise (Thornton et al. 1999; Smyser and Neil 2015; Liu et al. 2016; Goksan et al. 2017; Neil and Smyser 2018; Kaplan et al. 2022). As a result of these factors, the optimal sequences and processing streams for neonates versus older samples are different. In this study, we chose to optimize methods for each group rather than use a one-size-fits all approach; in our opinion this latter approach would exacerbate methodological problems because it would result in lower quality data from one of the groups. As a result of the above considerations, comparisons of functional connectivity between neonates and older samples likely reflect a combination of biological and methodological differences. Nevertheless, it is instructive to compare functional connectivity across groups as a means of providing an empirical explanation for why, e.g. neonates appear to have less well-connected networks, even as we work to identify which of these differences are methodological versus biological. In addition, variation in neonatal functional connectivity has been linked to factors such as preterm birth (Smyser et al. 2016; Rogers et al. 2017), socio-economic status (Ramphal et al. 2020), and drug and alcohol use in-utero (Roos et al. 2021); and functional properties at birth have been associated with outcomes in the first 2 years of life including symptoms related to anxiety (Graham et al. 2016; Rogers et al. 2017; Sylvester et al. 2017; Graham et al. 2019; Sylvester et al. 2021) and attention problems (Ramphal et al. 2020). To address these issues, in the current study children were full-term and had no known drug or alcohol exposures (maternal marijuana use was not excluded), and so future studies are required to determine, which aspects of neonatal brain organization are influenced by these factors.

In summary, the current study supports the hypothesis that adult-like functional relationships are detectable near birth. Key long-range anterior–posterior functional connections that typify the DMN, DAN, and FPN are exhibit network-selectivity in term-born neonates. These observations provide a foundation for studies of human brain development and for studies that seek to relate variation in brain development to variation in outcome.

Acknowledgments

The authors thank Joshua S. Shimony (J.S.S.) for reviewing the structural MRIs for neonatal injuries; and Karen Lukas and Rich Nagel for assistance with scanning.

Supplementary data

Supplementary material is available at *Cerebral Cortex online*.

Funding

This research was supported by National Institute of Health (grant nos. K23 MH109983 to C.M.S., R01 MH122389 to C.M.S., K02 NS089852 to C.D.S., R01 MH113570 to C.D.S. and C.E.R., R01 MH113883 to C.D.S. and J.L.L., P50 HD103525 to C.D.S., C.E.R., K23 MH105179 to C.E.R., R01 MH090786 to D.M.B., R01 MH096773 to D.A.F., R01 MH115357 to D.A.F., UG3 OD023349 to D.A.F. and A.M.G, and R34 DA050291 to D.A.F. and A.M.G); the McDonnell Center for Systems Neuroscience (C.M.S.); the Taylor Family Institute (C.M.S.); the Parker Fund

(C.M.S.); and the Masonic Institute for the Developing Brain (D.A.F.).

Conflict of interest statement: The authors report no additional conflicts of interest.

References

Adamson CL, Alexander B, Ball G, Beare R, Cheong JLY, Spittle AJ, Doyle LW, Anderson PJ, Seal ML, Thompson DK. Parcellation of the neonatal cortex using Surface-based Melbourne Children's Regional Infant Brain atlases (M-CRIB-S). *Sci Rep*. 2020:10:4359.

Alexander B, Murray AL, Loh WY, Matthews LG, Adamson C, Beare R, Chen J, Kelly CE, Rees S, Warfield SK, et al. A new neonatal cortical and subcortical brain atlas: the Melbourne children's regional infant brain (M-CRIB) atlas. *NeuroImage*. 2017:147:841–851.

Biswal B, Yetkin FZ, Haughton VM, Hyde JS. Functional connectivity in the motor cortex of resting human brain using echo-planar MRI. *Magn Reson Med*. 1995:34:537–541.

Brody BA, Kinney HC, Kloman AS, Gilles FH. Sequence of central nervous system myelination in human infancy. I. An autopsy study of myelination. *J Neuropathol Exp Neurol*. 1987:46:283–301.

Cao M, He Y, Dai Z, Liao X, Jeon T, Ouyang M, Chalak L, Bi Y, Rollins N, Dong Q et al. Early development of functional network segregation revealed by connectomic analysis of the preterm human brain. *Cereb Cortex*. 2017:27:1949–1963.

Cohen S, Williamson G. *Perceived stress in a probability sample of the United States*. Newbury Park, CA: Sage; 1988

Collin G, van den Heuvel MP. The ontogeny of the human connectome: development and dynamic changes of brain connectivity across the life span. *Neuroscientist*. 2013:19:616–628.

Cox JL, Holden JM, Sagovsky R. Detection of postnatal depression. Development of the 10-item Edinburgh Postnatal Depression Scale. *Br J Psychiatry*. 1987:150:782–786.

Dale AM, Fischl B, Sereno MI. Cortical surface-based analysis. I. Segmentation and surface reconstruction. *Neuroimage*. 1999:9: 179–194.

De Asis-Cruz J, Bouyssi-Kobar M, Evangelou I, Vezina G, Limperopoulos C. Functional properties of resting state networks in healthy full-term newborns. *Sci Rep*. 2015:5:17755.

Doria V, Beckmann CF, Arichi T, Merchant N, Groppo M, Turkheimer FE, Counsell SJ, Murgasova M, Aljabar P, Nunes RG et al. Emergence of resting state networks in the preterm human brain. *Proc Natl Acad Sci U S A*. 2010:107:20015–20020.

Dosenbach NUF, Koller JM, Earl EA, Miranda-Dominguez O, Klein RL, Van AN, Snyder AZ, Nagel BJ, Nigg JT, Nguyen AL et al. Real-time motion analytics during brain MRI improve data quality and reduce costs. *NeuroImage*. 2017:161:80–93.

Entringer S, Buss C, Wadhwa PD. Prenatal stress, development, health and disease risk: A psychobiological perspective-2015 Curt Richter Award Paper. *Psychoneuroendocrinology*. 2015:62:366–375.

Fair DA, Miranda-Dominguez O, Snyder AZ, Perrone A, Earl EA, Van AN, Koller JM, Feczko E, Tisdall MD, van der Kouwe A et al. Correction of respiratory artifacts in MRI head motion estimates. *NeuroImage*. 2020:208:116400.

Fischl B, Sereno MI, Dale AM. Cortical surface-based analysis. II: Inflation, flattening, and a surface-based coordinate system. *NeuroImage*. 1999:9:195–207.

Fox MD, Snyder AZ, Vincent JL, Corbetta M, Van Essen DC, Raichle ME. The human brain is intrinsically organized into dynamic, anticorrelated functional networks. *Proc Natl Acad Sci U S A*. 2005:102:9673–9678.

Fransson P, Skiöld B, Engström M, Hallberg B, Mosskin M, Aden U, Lagercrantz H, Blennow M. Spontaneous brain activity in the newborn brain during natural sleep–an fMRI study in infants born at full term. *Pediatr Res*. 2009:66:301–305.

Fransson P, Skiöld B, Horsch S, Nordell A, Blennow M, Lagercrantz H, Aden U. Resting-state networks in the infant brain. *Proc Natl Acad Sci U S A*. 2007:104:15531–15536.

Gao W, Alcauter S, Elton A, Hernandez-Castillo CR, Smith JK, Ramirez J, Lin W. Functional network development during the first year: relative sequence and socioeconomic correlations. *Cereb Cortex (New York, NY : 1991)*. 2015:25:2919–2928.

Gao W, Gilmore JH, Giovanello KS, Smith JK, Shen D, Zhu H, Lin W. Temporal and spatial evolution of brain network topology during the first two years of life. *PLoS One*. 2011:6:e25278.

Gao W, Gilmore JH, Shen D, Smith JK, Zhu H, Lin W. The synchronization within and interaction between the default and dorsal attention networks in early infancy. *Cereb Cortex (New York, NY : 1991)*. 2013:23:594–603.

Gao W, Lin W, Grewen K, Gilmore JH. Functional connectivity of the infant human brain: plastic and modifiable. *Neuroscientist*. 2016.

Gao W, Zhu H, Giovanello KS, Smith JK, Shen D, Gilmore JH, Lin W. Evidence on the emergence of the brain's default network from 2-week-old to 2-year-old healthy pediatric subjects. *Proc Natl Acad Sci U S A*. 2009:106:6790–6795.

Gilbert K, Perino MT, Myers MJ, Sylvester CM. Overcontrol and neural response to errors in pediatric anxiety disorders. *J Anxiety Disord*. 2020:72:102224.

Glasser MF, Sotiropoulos SN, Wilson JA, Coalson TS, Fischl B, Andersson JL, Xu J, Jbabdi S, Webster M, Polimeni JR et al. The minimal preprocessing pipelines for the Human Connectome Project. *NeuroImage*. 2013:80:105–124.

Goksan S, Hartley C, Hurley SA, Winkler AM, Duff EP, Jenkinson M, Rogers R, Clare S, Slater R. Optimal echo time for functional MRI of the infant brain identified in response to noxious stimulation. *Magn Reson Med*. 2017:78:625–631.

Gordon EM, Laumann TO, Adeyemo B, Huckins JF, Kelley WM, Petersen SE. Generation and ealuation of a cortical area parcellation from resting-state correlations. *Cereb Cortex*. 2016:26: 288–303.

Gordon EM, Laumann TO, Gilmore AW, Newbold DJ, Greene DJ, Berg JJ, Ortega M, Hoyt-Drazen C, Gratton C, Sun H et al. Precision functional mapping of individual human brains. *Neuron*. 2017:95: 791–807.e797.

Graham AM, Buss C, Rasmussen JM, Rudolph MD, Demeter DV, Gilmore JH, Styner M, Entringer S, Wadhwa PD, Fair DA. Implications of newborn amygdala connectivity for fear and cognitive development at 6-months-of-age. *Dev Cogn Neurosci*. 2016:18: 12–25.

Graham AM, Rasmussen JM, Entringer S, Ben Ward E, Rudolph MD, Gilmore JH, Styner M, Wadhwa PD, Fair DA, Buss C. Maternal cortisol concentrations during pregnancy and sex-specific associations with neonatal amygdala connectivity and emerging internalizing behaviors. *Biol Psychiatry*. 2019:85:172–181.

Grayson DS, Fair DA. Development of large-scale functional networks from birth to adulthood_ A guide to the neuroimaging literature. *NeuroImage*. 2017:1–0.

Greicius MD, Krasnow B, Reiss AL, Menon V. Functional connectivity in the resting brain: a network analysis of the default mode hypothesis. *Proc Natl Acad Sci U S A*. 2003:100:253–258.

Hill J, Inder T, Neil J, Dierker D, Harwell J, Van Essen D. Similar patterns of cortical expansion during human development and evolution. *Proc Natl Acad Sci U S A*. 2010:107:13135–13140.

Kamps FS, Hendrix CL, Brennan PA, Dilks DD. Connectivity at the origins of domain specificity in the cortical face and place networks. *Proc Natl Acad Sci U S A*. 2020:117:6163–6169.

Kaplan S, Meyer D, Miranda-Dominguez O, Perrone A, Earl E, Alexopoulos D, Barch DM, Day TKM, Dust J, Eggebrecht AT et al. Filtering respiratory motion artifact from resting state fMRI data in infant and toddler populations. *NeuroImage*. 2022:247: 118838.

Keunen K, Counsell SJ, Benders M. The emergence of functional architecture during early brain development. *NeuroImage*. 2017:160:2–14.

Kind AJH, Buckingham WR. Making neighborhood-disadvantage metrics accessible - the neighborhood atlas. *N Engl J Med*. 2018:378:2456–2458.

Laumann TO, Gordon EM, Adeyemo B, Snyder AZ, Joo SJ, Chen M-Y, Gilmore AW, McDermott KB, Nelson SM, Dosenbach NUF et al. Functional system and areal organization of a highly sampled individual human brain. *Neuron*. 2015:87:657–670.

Li J, Osher DE, Hansen HA, Saygin ZM. Innate connectivity patterns drive the development of the visual word form area. *Sci Rep*. 2020:10:18039.

Liu P, Chalak LF, Krishnamurthy LC, Mir I, Peng SL, Huang H, Lu H. T1 and T2 values of human neonatal blood at 3 Tesla: dependence on hematocrit, oxygenation, and temperature. *Magn Reson Med*. 2016:75:1730–1735.

Lynch CJ, Power JD, Scult MA, Dubin M, Gunning FM, Liston C. Rapid precision functional mapping of individuals using multi-echo fMRI. *Cell Rep*. 2020:33:108540.

Marcus DS, Harms MP, Snyder AZ, Jenkinson M, Wilson JA, Glasser MF, Barch DM, Archie KA, Burgess GC, Ramaratnam M et al. Human Connectome Project informatics: quality control, database services, and data visualization. *NeuroImage*. 2013:80: 202–219.

Marcus DS, Harwell J, Olsen T, Hodge M, Glasser MF, Prior F, Jenkinson M, Laumann T, Curtiss SW, Van Essen DC. Informatics and data mining tools and strategies for the human connectome project. *Front Neuroinform*. 2011:5:4.

Mathur AM, Neil JJ, McKinstry RC, Inder TE. Transport, monitoring, and successful brain MR imaging in unsedated neonates. *Pediatr Radiol*. 2008:38:260–264.

Molloy MF, Saygin ZM. Individual variability in functional organization of the neonatal brain. *NeuroImage*. 2022:253:119101.

Neil JJ, Smyser CD. Recent advances in the use of MRI to assess early human cortical development. *J Magn Reson*. 2018:293: 56–69.

Norr ME, Hect JL, Lenniger CJ, Van den Heuvel M, Thomason ME. An examination of maternal prenatal BMI and human fetal brain development. *J Child Psychol Psychiatry*. 2021:62:458–469.

Perino MT, Myers MJ, Wheelock MD, Yu Q, Harper JC, Manhart MF, Gordon EM, Eggebrecht AT, Pine DS, Barch DM et al. Whole-brain resting-state functional connectivity patterns associated with pediatric anxiety and involuntary attention capture. *Biol Psychiatry*. 2021:1:229–238.

Perino MT, Yu Q, Myers MJ, Harper JC, Baumel WT, Petersen SE, Barch DM, Luby JL, Sylvester CM. Attention alterations in pediatric anxiety: evidence From behavior and neuroimaging. *Biol Psychiatry*. 2021:89.

Posse S, Wiese S, Gembris D, Mathiak K, Kessler C, Grosse-Ruyken ML, Elghahwagi B, Richards T, Dager SR, Kiselev VG. Enhancement of BOLD-contrast sensitivity by single-shot multi-echo functional MR imaging. *Magn Reson Med*. 1999:42:87–97.

Power JD, Cohen Alexander L, Nelson Steven M, Wig Gagan S, Barnes Kelly A, Church Jessica A, Vogel Alecia C, Laumann Timothy O, Miezin Fran M, Schlaggar Bradley L et al. Functional network organization of the human brain. *Neuron*. 2011:72:665–678.

Power JD, Mitra A, Laumann TO, Snyder AZ, Schlaggar BL, Petersen SE. Methods to detect, characterize, and remove motion artifact in resting state fMRI. *NeuroImage*. 2014:84:320–341.

Raichle ME. The restless brain. *Brain connectivity*. 2011:1:3–12.

Ramphal B, Whalen DJ, Kenley JK, Yu Q, Smyser CD, Rogers CE, Sylvester CM. Brain connectivity and socioeconomic status at birth and externalizing symptoms at age 2 years. *Dev Cogn Neurosci*. 2020:45:100811.

Rogers CE, Sylvester CM, Mintz C, Kenley JK, Shimony JS, Barch DM, Smyser CD. Neonatal amygdala functional connectivity at rest in healthy and preterm infants and early internalizing symptoms. *J Am Acad Child Adolesc Psychiatry*. 2017:56: 157–166.

Roos A, Fouche JP, Ipser JC, Narr KL, Woods RP, Zar HJ, Stein DJ, Donald KA. Structural and functional brain network alterations in prenatal alcohol exposed neonates. *Brain Imaging Behav*. 2021:15: 689–699.

Rosvall M, Bergstrom CT. Maps of random walks on complex networks reveal community structure. *Proc Natl Acad Sci U S A*. 2008:105:1118–1123.

Shi F, Salzwedel AP, Lin W, Gilmore JH, Gao W. Functional brain parcellations of the infant brain and the associated developmental trends. *Cerebral cortex (New York, NY : 1991)*. 2017:1–11.

Smith SM, Jenkinson M, Woolrich MW, Beckmann CF, Behrens TE, Johansen-Berg H, Bannister PR, De Luca M, Drobnjak I, Flitney DE et al. Advances in functional and structural MR image analysis and implementation as FSL. *NeuroImage*. 2004:23(Suppl 1): S208–S219.

Smyser CD, Inder TE, Shimony JS, Hill JE, Degnan AJ, Snyder AZ, Neil JJ. Longitudinal analysis of neural network development in preterm infants. *Cereb cortex (New York, NY : 1991)*. 2010:20: 2852–2862.

Smyser CD, Neil JJ. Use of resting-state functional MRI to study brain development and injury in neonates. *Semin Perinatol*. 2015:39: 130–140.

Smyser CD, Snyder AZ, Shimony JS, Mitra A, Inder TE, Neil JJ. Resting-state network complexity and magnitude are reduced in prematurely born infants. *Cerebral cortex (New York, NY : 1991)*. 2016:26: 322–333.

Stiles J, Jernigan TL. The basics of brain development. *Neuropsychol Rev*. 2010:20:327–348.

Sylvester CM, Myers MJ, Perino MT, Kaplan S, Kenley JK, Smyser TA, Warner BB, Barch DM, Pine DS, Luby JL et al. Neonatal brain response to deviant auditory stimuli and relation to maternal trait anxiety. *Am J Psychiatry*. 2021:appiajp202020050672.

Sylvester CM, Smyser CD, Smyser T, Kenley J, Ackerman JJ, Shimony JS, Petersen SE, Rogers CE. Cortical Functional Connectivity Evident After Birth and Behavioral Inhibition at Age 2. *Am J Psychiatry*. 2017:appiajp201717010018.

Sylvester CM, Yu Q, Srivastava AB, Marek S, Zheng A, Alexopoulos D, Smyser CD, Shimony JS, Ortega M, Dierker DL et al. Individual-specific functional connectivity of the amygdala: A substrate for precision psychiatry. *Proc Natl Acad Sci U S A*. 2020:117:3808–3818.

Talairach J, Tournoux P. *Co-planar stereotaxic atlas of the human brain*. New York: Thieme; 1988

Tau GZ, Peterson BS. Normal development of brain circuits. *Neuropsychopharmacology*. 2010:35:147–168.

Thomason ME. Development of Brain Networks In Utero: Relevance for Common Neural Disorders. *Biol Psychiatry*. 2020:88:40–50.

Thomason ME, Hect JL, Waller R, Curtin P. Interactive relations between maternal prenatal stress, fetal brain connectivity, and

gestational age at delivery. *Neuropsychopharmacology*. 2021:46: 1839–1847.

Thornton JS, Amess PN, Penrice J, Chong WK, Wyatt JS, Ordidge RJ. Cerebral tissue water spin-spin relaxation times in human neonates at 2.4 tesla: methodology and the effects of maturation. *Magn Reson Imaging*. 1999:17:1289–1295.

Turk E, van den Heuvel MI, Benders MJ, de Heus R, Franx A, Manning JH, Hect JL, Hernandez-Andrade E, Hassan SS, Romero R et al. Functional connectome of the fetal brain. *J Neurosci*. 2019:39: 9716–9724.

van den Heuvel MI, Hect JL, Smarr BL, Qawasmeh T, Kriegsfeld LJ, Barcelona J, Hijazi KE, Thomason ME. Maternal stress during pregnancy alters fetal cortico-cerebellar connectivity in utero and increases child sleep problems after birth. *Sci Rep*. 2021:11:2228.

van den Heuvel MP, Kersbergen KJ, de Reus MA, Keunen K, Kahn RS, Groenendaal F, de Vries LS, Benders MJ. The neonatal connectome during preterm brain development. *Cereb Cortex*. 2015:25:3000–3013.

Van Essen DC, Glasser MF, Dierker DL, Harwell J, Coalson T. Parcellations and hemispheric asymmetries of human cerebral cortex analyzed on surface-based atlases. *Cereb Cortex*. 2012:22: 2241–2262.

Zhang H, Shen D, Lin W. Resting-state functional MRI studies on infant brains: A decade of gap-filling efforts. *NeuroImage*. 2019:185:664–684.